Nitrogen-vacancy nanodiamond based local thermometry using frequency-jump modulation

NV-nanodiamond based local thermometry using frequency-jump modulation

To cite this article before publication: Shashi Kanth Reddy Singam *et al* 2019 *Nanotechnology* in press https://doi.org/10.1088/1361-6528/ab5a0c

IOP Publishing Journal Title
Journal **XX** (XXXX) XXXXXX https://doi.org/XXXX/XXXX

NV-nanodiamond based local thermometry using frequency-jump modulation

Shashi K.R. Singam,[1] Milos Nesladek[2] and Etienne Goovaerts[*,1]

[1] Physics Department, University of Antwerp, Universiteitsplein 1, BE-2610 Antwerp, Belgium
[2] Institute for Materials Research (IMO), University Hasselt Wetenschapspark 1, BE-3590 Diepenbeek, Belgium

E-mail: Etienne.Goovaerts@uantwerp.be

Received xxxxxx
Accepted for publication xxxxxx
Published xxxxxx

Abstract

A straightforward and sensitive approach is presented for contact-free thermal sensing with high spatial resolution based on optically detected magnetic resonance (ODMR) of negatively charged nitrogen-vacancy (NV) centers in fluorescent nanodiamonds (FNDs). The frequency-jump procedure is a frequency modulation technique between two discrete frequencies at the inflection points at both sides of the NV ODMR resonance, which yields a signal proportional to the temperature shift over a wide temperature range. The approach is generic and is demonstrated by time-dependent measurements of the local temperature at different spots on a microelectronics circuit under electrical switching operation of one of the devices.

Keywords: term, term, term

1. Introduction

Negatively charged nitrogen-vacancy (NV) centers in (nano)diamond have in recent years been at the focus of research for potential applications ranging from optically addressable qubits, to fluorescent markers for biological microscopy, to nanoscale sensing of polarity, magnetic or electrical fields, as well as nuclear magnetic resonance (NMR) [1]-[4]. The temperature dependence of the NV^- electronic properties was initially considered as a detrimental effect, posing a limit to the performance in various applications [5],[6]. Soon, however, opportunities were recognized for the development of sensitive thermometry at the nanoscale [7],[8]. It was demonstrated that NV^- thermometry can be applied over a large temperature range [7],[8] while it can also detect minute temperature changes [8]-[12]. Various approaches have been followed with NV^- defects implanted in chips, in diamond tips used as scanning probes, as well as in dispersed fluorescent nanodiamonds (FND), mainly in biological applications [13]. These were fruitfully combined with microscopic imaging in different modes [12]-[16].

The NV^- defect in diamond is a nonblinking, highly efficient fluorescence center. It displays trigonal C_{3v} point symmetry and the $^3A_2$ ground state of the defect is a spin triplet. The latter exhibits a zero-field splitting (ZFS) of $D = 2.87$ GHz between the $m_S = 0$ and $m_S = \pm 1$ spin sub-levels, mainly resulting from magnetic dipole-dipole interaction. Excitation to an higher ^3E state yields photoluminescence (PL) with zero-phonon line at 638 nm and a broad phonon sideband towards the near infrared. The PL quantum efficiency is dependent on the initial spin state because of spin-selective intersystem crossing (ISC) between the ground and excited triplet states and intermediate energy singlet states, from which decay is nonradiative. The $m_S = 0 \rightarrow \pm 1$ spin transitions around 2.87 MHz are efficiently detected via changes in the PL intensity, by so-called optically detected magnetic resonance (ODMR), applicable to NV^- ensembles as well as to a single defect. The ZFS decreases with increasing

temperature reported by Acosta *et al.* [5],[6] with a specific shift around room temperature of

$$c_T = \frac{dD}{dT} = -74.2\ \text{kHz/K} \quad , \qquad (1)$$

which has been ascribed to the combined effects of lattice expansion and change in electron-phonon interactions [17]. The narrow linewidth of the ODMR transition combined with an important contrast in PL intensity at resonance is the basis for very sensitive temperature measurements (down to 5 mK/$\sqrt{Hz}$ for a single NV- in bulk diamond [10]) using continuous-wave (CW) or pulsed microwaves to manipulate the spins.

Here, we present a novel and straightforward approach to sensitively detect temperature shifts using the NV^- centers. The procedure is first demonstrated for subsurface NV^- centers in a diamond single crystal (SC). Then, sensing of heat dissipation is applied to a microelectronic circuit using FNDs dispersed on its surface, detecting the time-dependence temperature at different positions with respect to the powered electronic device. This generic method, which is based on the resonance frequency shift of the ODMR-detected NV^- spin resonance, is straightforward in its implementation and holds perspective for further improvement of sensitivity as well as for spatial mapping of the temperature.

2. Methods and Materials

The home-built microscope setup, described in more detail in Ref. [18], is used either as an inverted microscope, for the test measurements on SC diamond, or in a horizontal configuration, for detection of the FNDs dispersed on the device. In the latter configuration, the sample area is more accessible and space is available for mounting of the microelectronic device with external contact wires. In any of the configurations the sample can be excited by means of a frequency-doubled Nd:YAG laser (532 nm, Changchun New Industries Optoelectronics Tech. Co., Ltd., MLL-III-532–200 mW). An intensified charge-coupled-device camera (Stanford Computer Optics, Inc., 4 Quik E camera, 752×582) is used for observation and image collection. The emitted light can be redirected either into a compact spectrometer (Maya2000 Pro, Ocean Optics) for spectral analysis or delivered onto an avalanche photodiode (Hamamatsu C5460-01). Selective detection of NV emission is possible with a long-wavelength pass filters (630 nm) in imaging mode as well as for ODMR detection. In addition a short wave pass filter (710 nm) was used to eliminate backround emission from the III-V materials in the microlectronics chip.

Microwaves are emitted by a broadband antenna consisting of a loop of 1 mm diameter defined on an electronic board connected in series with a 50-Ω load. In the SC test experiments, the antenna loop was positioned at minimal distance behind the sample to maximize impinging microwave power, allowing the use of a 40x immersion-type objective. For probing of FNDs dispersed on the device, the antenna stood in front of the sample with the excitation and the collection of the PL performed through a ~1mm diameter aperture in the middle of the antenna loop. This had to stay at 1-2 mm from the target to ensure the integrity of the bonding wires contacting the individual devices. This configuration imposed a larger working distance, obtained with a 20x objective. The microwaves are provided by a combination of a signal generator (Rhode & Schwarz, SMC100A) and a microwave amplifier (WanTcom, Inc., WBPA2736A, 24 dB, max. 33-dBm).

The measurements presented here were performed at 27 dBm microwave power into the antenna circuit and and up to 1 mW laser power focused on the sample, which was chosen to optimize the ODMR contrast [18].

The CW ODMR spectrum was obtained by direct detection of the change in PL intensity. For temperature sensing, lock-in detection (EG&G, Princeton Applied Research, model 5204) is applied in combination with a modulation scheme in which the the generator is abruptly switching between two microwave frequencies, further referred to as frequency-jump modulation. In this mode, the maximum possible modulation rate afforded by the generator is 43 Hz. All frequency scans reported below are performed in 1 MHz steps with 1 s integration time. The time dependent measurements of the frequency-jump signal were recorded with 0.1s time steps. The lock-in time constant was 0.3 s, except when explicitly indicated otherwise.

The diamond single crystal used for initial testing was described in detail in Ref. [18]. FNDs of average size of 40 nm were obtained from Adámas Nanotechnologies prepared in aqueous suspension, which was directly used for drop casting on the microelectronic circuit.

For a controlled increase of the temperature in the test measurements on the SC, heat is applied by passing a current through a thin metal wire resistor placed close to the sample. In the application with FNDs dispersed on the microelectronic circuit, heat is locally dissipated by an electrical current sent through one of the AlAs/GaAs resonant tunneling devices on the chip, which is connected via bonding wires. This device consists of a square mesa (200 x 200 μm^2) composed of GaAs and thin barrier layers of AlAs grown by MBE, topped with a ohmic metal contact and surrounded by the GaAs substrate.

3. Results

When the local temperature at the NV^- centers changes, the ODMR resonance shifts in frequency according to Eq. 1, which is schematically illustrated in Figure 1(a). However, monitoring the local temperature by repeated measurements of this spectrum would be unacceptably slow an unpractical, and often unreliable due to drifts during the registration period. Therefore, an alternative approach is needed to monitor small and sudden temperature changes, based on a

signal that is very sensitive to frequency shifts of the resonance and can be measured in real time.

3.1. Frequency-jump modulation technique

The inflection points ν_1 and ν_2 (see Figure 1(a)) are the points of maximum slope in the fluorescence intensity *vs.* microwave frequency around the resonance, and thus also the points of highest intensity response to a shift in resonance frequency. This was also the basis for sensitive detection in magnetometry by means of frequency-modulation around one of these inflection points, as discussed in detail by Ma *et al.* [19]. Detection of the intensity change $I_i' - I_i$ at one of these frequencies could be envisaged as a measure of temperature change. However, the effect of the thermally induced frequency shift is then easily obscured by changes in the overall intensity due to e.g., intensity variations of the laser excitation or position drift of the laser spot over the fluorescent centers. A more suitable observable to probe the temperature is the intensity difference between the two inflection points $\Delta I = I_2 - I_1$. Besides doubling the sensitivity, this eliminates the influence of extrinsic background signals and strongly reduces the effects of variations in the NV^- fluorescence, but also in the resonance linewidth [20].

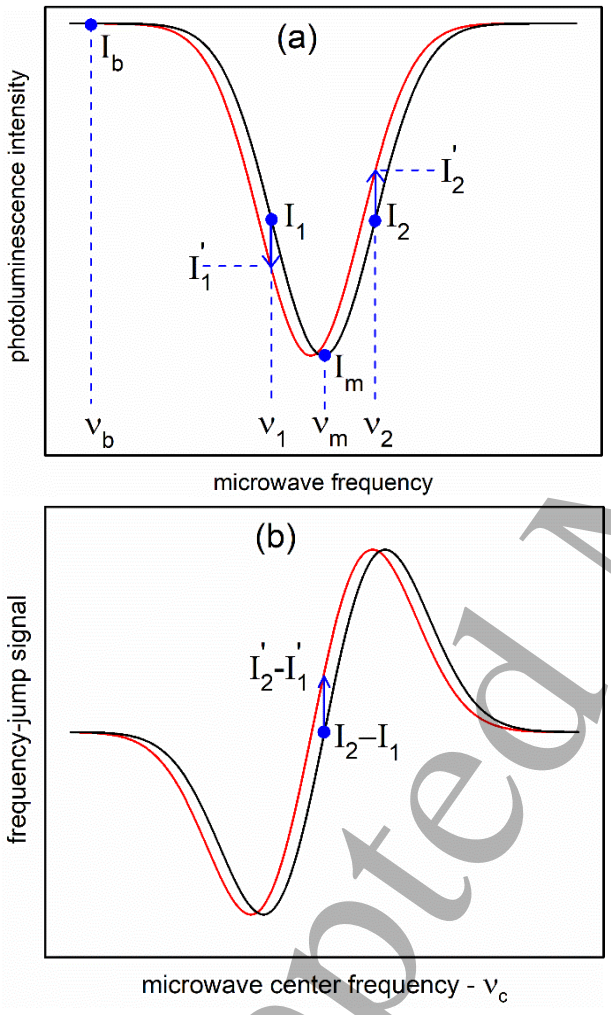

Figure 1: (a) Schematic representation of the dip in the PL-intensity due to the ODMR effect (idealized gaussian lineshape), shifting to lower frequency with temperature. The inflection points $\nu_{1,2}$ with corresponding intensities $I_{1,2}$ and $I'_{1,2}$, are indicated before and after warm up (black and red curves, respectively). The minimum and baseline intensities I_m and I_b at ν_m and ν_b, respectively, are useful for correction purposes. (b) Frequency-jump signal derived from the described modulation procedure, before ($\Delta I = I_2 - I_1$) and after ($\Delta I' = I_2' - I_1'$) temperature increase, as a function of center frequency $\nu_c = (\nu_1 + \nu_2)/2$.

Therefore we introduce an approach essentially different from the conventional frequency modulation. The frequency-jump technique, as the name suggests, consists of periodic jumping in frequency between the two inflection points in the CW ODMR spectrum, ν_1 and ν_2 (see Figure 1(a)). In our set-up a maximum jumping rate of 43 Hz is available, which is well below the limit set by the spin population relaxation time $T_1 \approx 6$ ms of the NV^- centers [21]. This periodic switching can be treated as a modulation and allows introduction of lock-in detection for efficient elimination of noise. The resulting error signal is essentially proportional to the change in local temperature for frequency shifts much smaller than the ODMR linewidth. This provides a reliable real-time observable for the frequency shift, *i.e.* for the variation in temperature. Let us now consider the expected error signal in function of the center frequency $\nu_c = (\nu_1 + \nu_2)/2$, as depicted in Figure 1(b) for the model gaussian lineshape. A striking feature is the quasi-linear region of this signal around the zero crossing, which results from the compensation of nonlinear effects up to third order in the frequency deviation, not only for a gaussian lineshape but for any functional form that is even with respect to the line position. A thermally induced frequency shift of the ODMR resonance is thus reflected in a proportional shift of this error signal spectrum, affording an efficient way to calibrate the temperature difference.

The ODMR resonance for FNDs deposited on the surface of a microelectronics device is shown in Figure 2(a), displaying unresolved strain-induced splitting of the transition. The corresponding experimental frequency-jump signal ΔI (Figure 2(b); $\nu_2 - \nu_1 = 28$ MHz) as a function of center frequency ν_c displays splittings in the side peaks related to the strain-induced splitting in the ODMR spectrum. This shape is closely agreeing with the one calculated from the strain-splitted ODMR spectrum taking the intensity difference between points ν_1 and ν_2 as a function of $\nu_c = (\nu_1 + \nu_2)/2$ (Figure 2(b), dotted). An essential feature is the quasi-linear region around the resonance frequency (see also inserted graph). The width of nearly 10 MHz of this region corresponds to a possible detection range of more than 100 K in temperature. The signal is measured before (black curve) and during heat dissipation in the device (red curve), which causes a small shift to lower frequency. Using Eq. 1, the shift

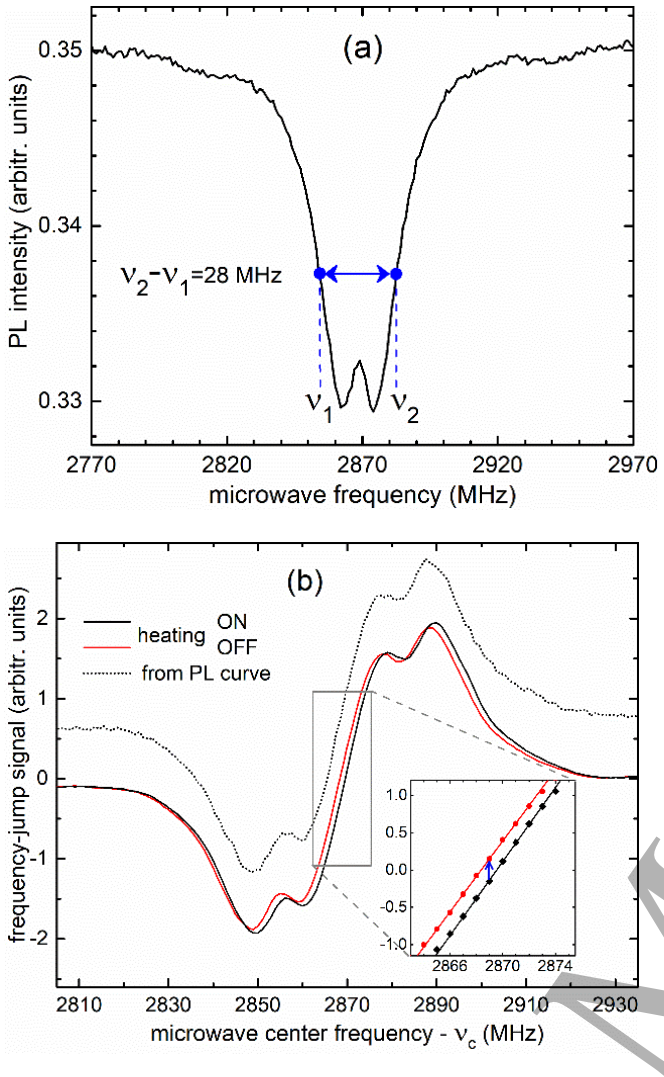

Figure 2: (a) ODMR resonance in the PL-intensity from FNDs deposited on a microelectronics device. The frequency difference between the inflection points is indicated. (b) Experimental frequency-jump spectrum before (black curve) and after (red curve) heating.The frequency shift, corresponding to a temperature increase ΔT = 15.7 K, is zoomed out in the insert and shown together with best linear fits and the change in frequency-jump signal (blue arrow). The dotted line (vertically scaled and shifted) is calculated from the ODMR spectrum in (a).

affords a calibration of the temperature difference, amounting to $\Delta T = 7.8$ K, that is more accurate and reliable than using the shift of the ODMR spectrum. Based on this calibration, the change in temperature can now be monitored by the error signal at a fixed frequency close to resonance as also illustrated in 2(b) (see insert, blue arrow).

Monitoring of the temperature is presented in Figure 3(a) for the case of NV^- defects in a diamond SC, showing exponential transients after switching on the heating (black curve) and, allowing a few minutes in between for thermalization, after switch-off (red curve, translated in time), with an characteristic (1/e) time of ~13 s in both cases. This is ascribed to heating and cooling of the crystal as a whole, considering the high thermal conductivity of diamond, in thermal exchange with its surroundings. The high signal-to-noise ratio combined with the calibration of the total temperature change sets an uncertainty below 0.5 K on the temperature shifts over a available range up to several tens of kelvin. The curves also show sudden changes in temperature affording subsecond time resolution (see below).

3.2. Measuring heat diffusion in a microelectronic circuit

Having demonstrated the working principle of the frequency-jump technique, we now proceed to its application in local thermometry on a microelectronic circuit. Figure 3(b) shows the transient signal from FNDs deposited on the electrode of a device (see Figure 4(a)) in which heat is dissipated by the operation of this very device, selected by

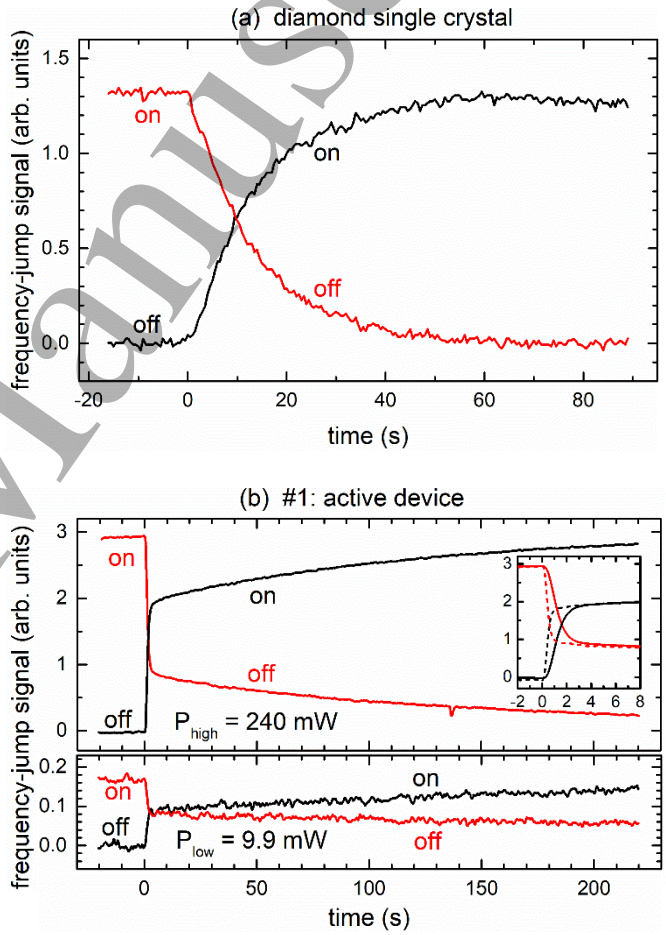

Figure 3: (a) Time dependence of the NV^- frequency-jump signal, revealing the change in local temperature in a single crystal under heating with a resistive wire in its close vicinity, after sudden switch on (black) and off (red). Here, the overall change in temperature is ΔT = 7.8 K, with a response (1/e) time of 13 s. (b) Corresponding curves for the signal from FNDs deposited on the active device (spot #1) after switching the current through this device at high (top) and low (bottom) dissipated power levels of P_{high} = 230 mW (90 mA / 2.6 V) and P_{low} = 9.9 mW (11.9 mA / 0.91 V). The corresponding overall temperature changes are ΔT_{tot} = 35.7 K and 2.1 K, respectively. The insert in (b) shows the initial fast steps, with the solid and broken curves for lock-in integration time set at 0.1 and 0.3 s, respectively.

position of the focused exciting laser beam in spot #1. As in the SC case, the device is suddenly switched on in a first measurement (black curve), while after a long thermalization period it is switched off in a second measurement (red curve), and this was repeated for two conditions of operation applying high (P_{high} = 230 mW, 90 mA/2.6 V) and low (P_{low} = 9.9 mW, 11.9 mA / 0.91 V) heating power levels, respectively. From the frequency dependence at steady state without and with heating (see Figure 2(b)) the overall temperature difference was calibrated to be ΔT = 35.7 K for the high-power case, and proportionally ΔT = 2.1 K for the low-power case. The factor 17 between both is somewhat smaller than but close to the ratio of 23 between the applied power levels. Taking into account the noise level, the low-power experiment demonstrates a sensitivity in the 0.5 K range for the temperature changes of the device in the present measuring conditions.

Interestingly different from the SC results, the thermal response is now composed of two parts: a fast initial step followed by a much slower one evolving towards steady state. Reduction of the lock-in time constant from 0.3 s to 0.1 s demonstrates (see inset of Figure 3(b)) that the observed width of this initial step is limited by the response of the instrument. More fundamentally, the spin population relaxation time of the NV- center potentially limits the response time, but this can be alliviated using sufficiently high optical pumping rates of the NV^- defects, since this is limiting the memory time of the spin state.

The subsequent slow evolution is close to exponential with a time constant $\tau \cong 120$ s, which is the same after on or off switching of the current, i.e. the same for heating and cooling. This results in the mirror symmetry observed between these two curves around the average temperature shift. These characteristics are very similar for high and for low heating power.

The position dependence of the thermal response on the circuit could be studied by detection in additional spots on neighboring devices marked in the microscope picture in Figure 4(a). Simple drop casting from water solution was used

Table 1: Overall temperature change ΔT_{tot} under switching operation of the device at spot #1 (P_{high} = 230 mW, 90 mA at 2.6 V) split up between the initial fast step ΔT_{step} and the further change ΔT_{slow} ($= \Delta T_{tot} - \Delta T_{step}$) during the slow near exponential approach of the steady state (estimated error bars:

detection spot	ΔT_{tot} (K)	ΔT_{step} (K)	ΔT_{slow} (K)
#1	35.7	24.4	11.3
#2	17.6	7.5	10.1
#3	14.8	4.8	10.0
#3	12.6	4.0	8.6

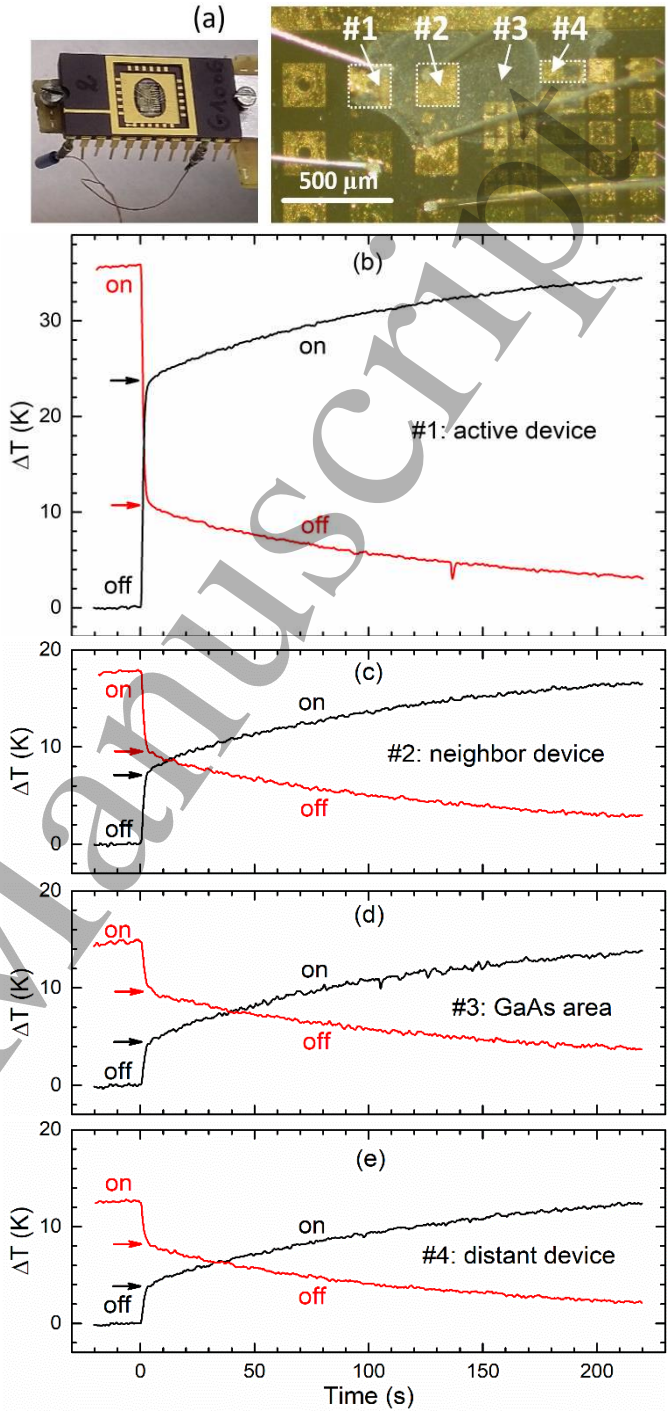

Figure 4: (a) Pictures of the microelectronics circuit and of the local lay-out on the chip showing the four probing spots for the time-dependent measurement, in which a whitish area with drop-cast FNDs can be discerned. The contact pads for the devices at spots #1 (with wire), #2 and #3 have been marked for clarity. (b-e) Temperature change under sudden switch on (black curves) or off (red curves) of the current through the device at spot #1 (P_{high} = 230 mW, 90 mA/2.6 V), comparing the four measuring spots. The horizontal arrows mark the point of transition from the near instantaneous initial step to the slow exponential part of the curves.

to deposition the FNDs, which is visible as a whitish stained area in the picture. This is quite sufficient for our present purpose, although more homogeneous FND deposition could be reached by other techniques (e.g., adjusting solvent, or using spray coating). The effect of on- and off-switching under P_{high} in the device at spot #1 were monitored by local measurements at three additional positions at increasing distance from the active device: a neighbor device (#2), an intermediate GaAs area (#3), and a more distant device (#4). Each time, a specific spot is selected by positioning of the focused exciting laser beam.

Figure 4(b) shows the results already discussed earlier (Figure 3(b), P_{high}) for detection at spot #1, but now after calibration for direct reading of changes in temperature. [§] This can now be compared with the corresponding traces detected on the neighboring devices (Figures 4(b-e)). While the general characteristics are the same, clearly the relative importance of the step and slow components is changing: while in the active device (#1) the step is dominant, this is strongly decreasing in the more remote spots (see ΔT values in Table 1). While the slow temperature change is somewhat decreasing in the series from #1 to #4, this is a limited trend. Shifting the curves vertically, the slow parts ot the traces for the three spots can nearly be overlayed showing the same characteristic time dependence with common response time. Clearly, the fast component possesses a sharp spatial profile with radius of the order of the distance between devices. It is followed by a slow component in the time evolution distributed over a much larger area, which lasts until the heat flow from the chip to the environment equals the locally dissipated power. A detailed description of this heating process requires additional investigation and analysis. However, the results clearly demonstrate the value of the frequency-jump approach for local thermometry.

4. Discussion and Conclusions

We have presented the frequency-jump procedure for NV^- based contactless local thermometry and demonstrated its feasibility in the study of heat dissipation in a microelectronics circuit. The method is however generic for various sensing applications based on the shift of an ODMR resonance line of the NV^- center in (nano)diamond, e.g. magnetometry or detection of local electrical fields. We implemented the technique using continuous-wave microwave excitation, but the principle can be immediately transposed to detection in pulsed mode, with the known advantages.

At this point, it is worth to consider possible improvement of the method and envisage its extension to thermal imaging. Indeed, the temperature measurement and its calibration are in the present implementation prone to fluctuation in the collected emission, which could result among other reasons from drift in position of the laser spot and variation of the FND density on the sample. Evidently, the detected difference $\Delta I = I_2 - I_1$ is proportional to the overall intensity of NV^- fluorescence, which calls for normalization of the error signal. However, the fluorescence may in the same wavelength range as the NV^- emission contain unwanted contributions from the sample, from specific materials involved (e.g. in this circuit from III-V semiconductors), from other fluorescent defects in the FNDs or from contamination. This can be avoided by selective calibration to the resonant part of the emission, i.e. the difference $I_b - I_m$ between the intensity at a frequency ν_b far enough from the ODMR-induced dip, and the minimal one the resonance frequency ν_m (see Figure 1(a)). Using the normalized quantity $(I_2 - I_1)/(I_b - I_m)$ will minimize the effects of intensity fluctuations due to laser or position drift. Moreover, in given conditions of microwave and laser excitation, the calibration will then be unchanged for different positions in the sample or between subsequent samples. This improvement can be implemented by programmed jumping of the microwave frequency between the four mentionned positions, with synchronuous sampling and processing, which is quite straightforward at the required repetition rate in the required range. [§§]

Although technically more challenging, the 4-points frequency-jump technique is a suitable basis for extension to imaging applications. Read-out times of several milliseconds are available for sensitive 2D-detectors in range 630-800nm of the NV^- emission, and therefore the required frequency sequence can be performed at similar rates, but now for the whole image. Also, the parallel treatment of the pixels is not unrealistic for a performant real-time processor. Wide-field optical excitation of the NV^- centers in the microscope can be reached either by inserting a defocusing lens for the 532 nm laser beam, or by the introduction of a narrow band LED around 530 nm as alternative light source, which in both cases can be operated at sufficiently high power.

The frequency-jumping technique as described in this paper is an efficient and straightforward approach for real time (sub-second) applications of local (sub-µm) thermal (sub-Kelvin) probing, which can be performed on microelectronic chips as well as in other sytems. As discussed above, there are opportunities for improvement of the method in speed, accuracy and reliability, and also for an implementation adapted to thermal imaging.

Acknowledgements

The authors are grateful to P. Casteels for technical assistance, and B. Yavkin for contributions to the implementation of ODMR measurements. The authors acknowledge the Research Foundation Flanders (FWO - Vlaanderen) for support of this work through grant no. G.088812N, from which one of the authors (S.K.R. Singam) obtained a PhD scholarship, as well as grants no. G.0D5816N and S004018N. Also, the European Commision provided

support in the project ASTERIQs (#820394). We thank C. Van Hoof (Imec, Leuven, Belgium) for providing the electronic devices used in the experiments.

Notes and references

§ Heat dissipation by the probe laser is constant and small compared to the electrically dissipated power, taking also into account the reduction by reflection and scattering. While this does not influence the overal heating and cooling curves of interest here, a localized heating occurs within the laser spot (few μm diameter). Varying the laser power at spot #1 and extrapolation to zero leads to an estimated local temperature increase of 5K in this spot. Whenever such local temperature changes are considered important, the probing laser power should be reduced.

§§ It is worth mentioning here that alternative 3- and 4-point schemes have been previously proposed [14],[22], using a set of measurements at different microwave frequencies for accurate determination of the shift of the NV^- ODMR resonance in nanothermometry.

[1] R. Schirhagl, K. Chang, M. Loretz and C.L. Degen, *Annu. Rev. Phys. Chem.*, 2014, **65**, 83. Nitrogen-Vacancy Centers in Diamond: Nanoscale Sensors for Physics and Biology

[2] G. Balasubramanian, A. Lazariev, S.R. Arumugam and D.-w. Duan, *Curr. Opinion Chem. Biol.*, 2014, **20**, 69. Nitrogen-Vacancy color center in diamond — emerging nanoscale applications in bioimaging and biosensing

[3] J.-W. Zhou, P.-F. Wang, F.-Z. Shi, P. Huang, X. Kong, X.-K. Xu, Q. Zhang, Z.-X. Wang, X. Rong and J.-F. Du, *Front. Phys.*, 2014, **9**, 587. Quantum information processing and metrology with color centers in diamonds

[4] W.W.-W. Hsiao, Y.Y. Hui, P.-C. Tsai and H.-C. Chang, *Acc. Chem. Res.*, 2016, **49**, 400. Fluorescent Nanodiamond: A Versatile Tool for Long-Term Cell Tracking, Super-Resolution Imaging, and Nanoscale Temperature Sensing

[5] V.M. Acosta, E. Bauch, M.P. Ledbetter, A. Waxman, L.-S. Bouchard and D. Budker, *Phys. Rev. Lett.*, 2010, **104**, 070801. Temperature dependence of the nitrogen-vacancy magnetic resonance in diamond

[6] V.M. Acosta, A. Jarmola, L.J. Zipp, M.P. Ledbetter, E. Bauch and D. Budker, *Proc. of SPIE*, 2011, **7948**, 79480W. Broadband magnetometry by infrared-absorption detection of diamond NV centers and associated temperature dependence

[7] T. Plakhotnik and D. Gruber, *Phys. Chem. Chem. Phys.*, 2010, **12**, 9751. Luminescence of nitrogen-vacancy centers in nanodiamonds at temperatures between 300 and 700 K: perspectives on nanothermometry

[8] D.M. Toyli, D.J. Christle, A. Alkauskas, B.B. Buckley, C.G. Van de Walle and D.D. Awschalom, *Phys. Rev. X*, 2012, **2**, 031001. Measurement and Control of Single Nitrogen-Vacancy Center Spins above 600 K

[9] D.M. Toyli, C.F. de las Casas, D.J. Christle, V.V. Dobrovitski and D.D. Awschalom, *PNAS*, 2013, **110**, 8417. Fluorescence thermometry enhanced by the quantum coherence of single spins in diamond

[10] P. Neumann, I. Jakobi, F. Dolde, C. Burk, R. Reuter, G. Waldherr, J. Honert, T. Wolf, A. Brunner, J.H. Shim, D. Suter, H. Sumiya, J. Isoya and J. Wrachtrup, *Nano Lett.*, 2013, **13**, 2738. High-precision nanoscale temperature sensing using single defects in diamond

[11] T. Plakhotnik, M.W. Doherty, J.H. Cole, R. Chapman and N.B. Manson, *Nano Lett.*, 2014, **14**, 4989. All-Optical Thermometry and Thermal Properties of the Optically Detected Spin Resonances of the NV- Center in Nanodiamond

[12] J. Wang, F. Feng, J. Zhang, J. Chen, Z. Zheng, L. Guo, W. Zhang, X. Song, G. Guo, L. Fan, C. Zou C, L. Lou, W. Zhu and G. Wang, *Phys. Rev. B*, 2015, **91**, 155404. High-sensitivity temperature sensing using an implanted single nitrogen-vacancy center array in diamond

[13] S. Sotoma, C.P. Epperla and H.-C. Chang, *ChemNanoMat*, 2018, **2**, 15. Diamond Nanothermometry

[14] G. Kucsko, P.C. Maurer, N.Y. Yao, M. Kubo, H.J. Noh, P.K. Lo, H. Park and M.D. Lukin, *Nature*, 2013, **500**, 54. Nanometre-scale thermometry in a living cell

[15] J.-P. Tetienne, A. Lombard, D.A. Simpson, C. Ritchie, J. Lu, P. Mulvaney and L.C.L. Hollenberg, *Nano Lett.*, 2016, **16**, 326. Scanning Nanospin Ensemble Microscope for Nanoscale Magnetic and Thermal Imaging

[16] A. Laraoui, H. Aycock-Rizzo, Y. Gao, X. Lu, E. Riedo and C.A. Meriles, *Nature Comm.*, 2016, **6**, 8954. Imaging thermal conductivity with nanoscale resolution using a scanning spin probe

[17] M.W. Doherty, V.M. Acosta, A. Jarmola, M.S.J. Barson, N.B. Manson, D. Budker and L.C.L. Hollenberg, *Phys. Rev. B*, 2014, **90**, 041201. Temperature shifts of the resonances of the NV- center in diamond.

[18] S.K.R. Singam, J. Motylewski, A. Monaco, E. Gjorgievska, E. Bourgeois, M. Nesládek, M. Giugliano and E. Goovaerts, *Phys. Rev. Appl.*, 2016, **6**, 064013. Contrast induced by a static magnetic field for improved detection in nanodiamond uorescence microscopy

[19] Z. Ma, S. Zhang, Y. Fu, H. Yuan, Y. Shi, J. Gao, L. Qin, J. Tang, J. Liu and Y.Li, *Opt. Express*, 2018, **26**, 382. Magnetometry for precision measurement using frequency-modulation microwave combined efficient photon-collection technique on an ensemble of nitrogenvacancy centers in diamond

[20] A. Dréau, M. Lesik, L. Rondin, P. Spinicelli, O. Arcizet, J.-F. Roch and V. Jacques, *Phys. Rev. B*, 2011, **84**, 195204. Avoiding power broadening in optically detected magnetic resonance of single NV defects for enhanced dc magnetic field sensitivity

[21] A. Jarmola, V.M. Acosta, K. Jensen, S. Chemerisov and D. Budker, *Phys. Rev. Lett.*, 2012, **108**, 197601. Temperature- and magnetic-field-dependent longitudinal spin relaxation in nitrogen-vacancy ensembles in diamond

[22] Y.-K. Tzeng, P.-C. Tsai, H.-Y. Liu, O.Y. Chen, H. Hsu, F.-G. Yee, M.-S. Chang and H.-C. Chang, *Nano Lett.*, 2015, **15**, 3945. Time-Resolved Luminescence Nanothermometry with Nitrogen-Vacancy Centers in Nanodiamonds